Impermeable thin Al_2O_3 overlay for TBC protection from sulfate and vanadate attack in gas turbines

Final Report

Reporting Period Start Date: Sep. 1, 2001
Reporting Period End Date: Aug. 31, 2005
Principal Author: Scott X. Mao
Date Report was issued (Oct 30, 2005)
DOE Award Number: DE-FC26-01NT41189

Department of Mechanical Engineering
University of Pittsburgh
3700 O'Hara St.
Pittsburgh, PA 15261
smao@engr.pitt.edu, Tel: 412-624-9602

DISCLAIMER

ABSTRACT

In order to improve the hot corrosion resistance of conventional YSZ TBC system, a dense and continues overlay of Al_2O_3 coating of about 0.1 - 25 mm thick was deposited on the surface of TBC by EB-PVD, high velocity oxy-fuel (HVOF) spray and composite-sol-gel (CSG) techniques. Hot corrosion tests were carried out on the TBC with and without Al_2O_3 coating in molten salts mixtures (Na_2SO_4 + 5%V_2O_5) at 950^oC for 10h. The microstructures of TBC and overlay before and after exposure were examined by means of scanning electron microscopy (SEM), energy-dispersive X-ray spectrometer (EDX), X-ray diffraction (XRD) and secondary ion mass spectrometry (SIMS). In order to investigate the effect of Al_2O_3 overlay on degradation and spalling of the TBC, indentation test has been employed to study spallation behaviors of YSZ coating with and without Al_2O_3 overlay.

It has been found that TBC will react with V_2O_5 to form YVO_4 in hot corrosion tests. A substantial amount of M-phase of ZrO_2 was formed due to the leaching of Y_2O_3 from YSZ. During hot corrosion test, there were no significant interactions between overlay Al_2O_3 coating and molten salts. After exposure, the alumina coating, especially produced by HVOF, was still very dense and cover the surface of YSZ, although they had been translated to $a-Al_2O_3$ from original $g-Al_2O_3$. As a result, Al_2O_3 overlay coating decreased the penetration of salts into the YSZ and prevented the YSZ from the attack by molten salts containing vanadium. Accordingly, only a few M-phase was formed in YSZ TBC, compared with TBC without overlay coating. The penetration of salts into alumina coating was thought to be through microcracks formed in overlay Al_2O_3 coating and at the interface between alumina and zriconia due to the presence of tensile stress in the alumina coating. Al_2O_3 overlay acted as a barrier against the infiltration of the molten salt into the YSZ coating during exposure, thus significantly reduced the amount of M-phase of ZrO_2 in YSZ coating. However, a thick Al_2O_3 overlay was harmful for TBC by increasing compressive stress which causes crack and spalling of YSZ coating. As a result, a dense and thin Al_2O_3 overlay is critical for simultaneously preventing YSZ from hot corrosion and spalling.

TABLE OF CONTENTS

LIST OF GRAPHICAL MATERIALS

Table 1 Quantitatively comparison of vanadium content in the YSZ layer by SIMS

1. INTRODUCTION

Thermal barrier coatings (TBCs) are finding increased application in overall component design of gas turbine. TBCs reduce the severity of thermal transients and lower the substrate temperature, thus improving fuel economy, engine power and component durability in engines. Yttria-stabilized zirconia (YSZ) TBCs is widely used in aero gas turbines [1-2]. Attempts to bring the advantages of TBCs to industrial and marine engines have been limited, however, in part because YSZ coatings are degraded by the reaction of Yttria with traces of sodium, sulfur, and especially vanadium present in many industrial-quality fuels, although zirconia itself shows good resistance to the molten sulfate or vanadate compounds arising from fuel impurities [3-4]. The majority of present-day TBCs are 8% Y_2O_3-ZrO_2 type as they exhibiting superior performance in the absence of vanadium. The critical problem is that yttria reacts react with the V_2O_5 or $NaVO_3$ to form YVO_4 in the case of molten salt containing small amount of V_2O_5 as follows:

$$Y_2O_3\,(\text{in } ZrO_2) + V_2O_5\,(\text{in melt}) = 2\,YVO_4\,(\text{solid}) \qquad (1)$$

This reaction depletes the Y_2O_3 stabilizer from ZrO_2 matrix and causes destabilization (i.e., transformation of the zirconia from the tetragonal and/or cubic to monoclinic phase upon cooling, which is accompanied by a large destructive volume change.) and degradation of the YSZ coating. Destabilization of the TBCs eventually causes the delamination and spalling of the ceramics coating. In addition, molten salts can penetrate into the YSZ coatings along porous and cracks in YSZ TBC and react with the metallic bond coat.

Therefore, the proposed idea for preventing the YSZ coating system from hot corrosion is the development of a dense overlay on the outer surface of YSZ coating to isolate the YSZ coating system from the molten salts so that chemical or physical change of the YSZ coating does not occur.

Alumina (Al_2O_3) is a well-know oxide material that has diverse application as engineering ceramics. Alumina has a high melting point and stabilization without showing phase transition at high temperature like the ZrO_2 ceramics. In addition, Al_2O_3 has a small solubility particularly in molten salts and is expected to show an excellent corrosion resistance. Al_2O_3 layer on metallic substrate has exhibited a very important role against corrosion. This allows the potential application of Al_2O_3 in gas turbines. However, Al_2O_3 has relatively high thermal conductivity (0.02-0.06W/cmK) compared with YSZ. Therefore, in the present TBC design, the YSZ coating acts as a thermal barrier and the Al_2O_3 coating plays a role in preventing hot-corrosion.

In the present study, a high-purity Al_2O_3 overlay was deposited onto the surface of YSZ coating by means of EB-PVD, high velocity oxy-fuel (HVOF) spray and composite-sol-gel (CSG) techniques. Hot corrosion tests were carried out. By using XRD, SEM and EDX analyses, the microstructure, hot corrosion behaviors of the surface modified TBC system with alumina coating were described in comparison with the conventional TBC system.

However, due to the thermal expansion mismatch between YSZ coating and Al_2O_3 overlay, such surface modification using Al_2O_3 overlay might deteriorate strain tolerance of the TBC. In the present work, in order to investigate the effect of Al_2O_3 overlay on degradation and

spalling of the TBC, indentation test has been employed to study spallation behaviors of YSZ coating with and without Al_2O_3 overlay.

2. EXECUTIVE SUMMARY

Overlay of Al_2O_3 coating deposited by EB-PVD, HVOF and CSG is mainly consisted of g - Al_2O_3. The Al_2O_3 overlay was dense, continues and adherent to the TBC. Hot corrosion tests were done on TBC with and without the Al_2O_3. The results show that there were no significant interactions between overlay Al_2O_3 coating and molten salts. Al_2O_3 overlay coating can prevent the YSZ from the attack by molten salts containing vanadium and decrease the penetration of the salts into the YSZ TBC, although there were some cracks in alumina coating and at the interface between alumina and zirconia formed during the hot corrosion tests. Indenter test was employed to investigate the spalling of YSZ with and without Al_2O_3 overlay after hot corrosion. The results showed that a thick Al_2O_3 overlay was harmful for TBC by increasing compressive stress which causes crack and spalling of YSZ coating. As a result, a dense and thin Al_2O_3 overlay is critical for simultaneously preventing YSZ from hot corrosion and spalling.

3. EXPERIMENTAL

The TBC system used in this study consisted of 6061 nickel-based superalloy substrate, CoNiCrAlY alloy bond coat as well as zirconia-8%yttira (YSZ) ceramic top coating. The bond coat and the YSZ TBC were produced by LPPS and APS, with the thickness of 100 and 250 mm, respectively. After receiving the TBC samples, overlay Al_2O_3 coating was deposited by EB-PVD, HVOF and CSG techniques. The thickness of Al_2O_3 coating was approximately 0.1 - 30 mm.

In order to compare the hot corrosion resistance of the TBCs with and without Al_2O_3 coating, hot corrosion experiments were carried out. The samples were exposed to molten salts mixtures (Na_2SO_4 + 5%V_2O_5) by placing them into a still air furnace at 950^oC for 10h exposures. A Philips PW1700 series diffractometer was employed to perform the phase analysis. X-ray diffraction (XRD) was used to determine whether reaction had taken place. XRD patterns were first obtained from the samples (YSZ TBC and YSZ TBC/Al_2O_3 overlay) before exposure to the molten salt. After exposure, the samples were cooled down to room temperature in the furnace. The exposured samples were cleaned in distilled water. XRD analyses were then carried out to the exposured samples. The extent of destabilization (D) of the YSZ TBC was estimated by

$$\mathrm{D}\,(\%) = \frac{M}{T+M} \times 100 \qquad (2)$$

Where T is the height of the zirconia tetragonal (111) peak, and M is the height of the zirconia monoclinic $(1\bar{1}1)$ peak in XRD test. For the sample of TBC/Al_2O_3 overlay, in order to detect the same depth as that of TBC without Al_2O_3 overlay, XRD test was done again on the sample whose overlay Al_2O_3 coating has been removed.

The microstructures and composition changes on the coating surface and their cross-sections after hot corrosion tests were examined using scanning electron microscopy (SEM), energy-dispersive X-ray spectrometer (EDX) equipped in SEM and SIMS.

In order to investigate the effect of Al_2O_3 overlay on degradation and spalling of the TBC, high-purity Al_2O_3 overlays of 25 mm and 2 mm thick are deposited onto the surface of YSZ coating by means of HVOF) spray and CSG techniques, respectively. After exposure to air and

to molten Na_2SO_4 salt containing V_2O_5 at high temperature, in addition to examinations of microstructure and visual check of TBC spallation, indentation test has been employed to study spallation behaviors of YSZ coating with and without Al_2O_3 overlay.

4. RESULTS AND DISCUSSION

4.1 CHARACTERS OF MATERIALS

4.1.1 Conventional YSZ TBC

SEM micrographs of the cross-section and surface morphology of as-sprayed TBC, shown in Fig.1, indicated that the TBC had a typical APS microstructure [5] and contained predominantly T-phase of ZrO_2 (see A in Fig.6), with inter-splat porosity and complex pattern of microcracks. It was found that the thickness of the bond coat and YSZ was 100 mm and 250 mm, respectively. It was visible that there were microcracks and porous on the surface of the TBC, which are considered to be the path for molten salts to attack the TBC system.

4.1.2 TBC/EB-PVD overlay Al_2O_3 coating

Fig.2 shows the cross-section and surface SEM micrograph of the TBC with Al_2O_3 overlay coating sputtered by EB-PVD. It is seen that the Al_2O_3 coating is dense and adherent to the TBC. The thickness of the Al_2O_3 coating was estimated to be about 25 mm. The surface micrograph of as-deposited specimen revealed a 'cauliflower' type of structure or dome shaped. The XRD pattern of the specimen in the as-deposited condition (A in Fig.7) demonstrated that TBC contained predominantly T-phase and Al_2O_3 coating was mainly consisted of g -Al_2O_3. The broad g – Al_2O_3 peaks indicated either nanosize crystallites or stress within the overlay Al_2O_3 coating.

4.1.3 TBC/HVOF overlay Al_2O_3 coating

Fig.3 shows the cross-section and surface SEM micrograph of the TBC with Al_2O_3 overlay coating sprayed by HVOF technique. Al_2O_3 coating is also very dense and adherent to the TBC. The surface morphology of alumina overlay coating produced by HVOF was similar to that of ASP zirconia TBC layer, but the particle size was much smaller than that of TBC, probably due to the higher temperature and particle speed during HVOF deposit. Therefore, denser, non-cracks and continuous coating could be obtained. Al_2O_3 overlay coating sprayed by HVOF was comprised of g - Al_2O_3 and a little bit of a - Al_2O_3 (A in Fig.8).

4.1.4 TBC/CSG overlay Al_2O_3 coating

Thin and dense alumina overlay (60-1000 nm) has been successfully deposited on the surface of YSZ by the composite-sol-gel (CSG) dip coating route with dipping solution consisted of 30cm^3 of 1 mol dm^{-3} boehmite sol mixed with 20cm^3 aqueous polyvinyl alcohol (PVA) solution at a concentration of 3.5g per 100cm^3 and 5 g calcined a – Al_2O_3 particles (300 nm) followed by calcinations at 1200^{o}C. CSG alumina overlay remarkably refrained the infiltration of the molten salt into the YSZ coating. The amount of M-phase in the TBC coating with Al_2O_3 overlay was substantially reduced comparing to that without alumina overlay.

The secondary- electron and backscattered-electron morphologies of the YSZ surface after dip coating with boehmite sol followed by calcined at 1200^{o}C are shown in Fig.4. Fig.4(c)

shows that a microcrack of 0.5-1.0 mm width on the YSZ surface was filled and blocked by alumina particles whose size was in the range of 100-350nm. The dark regions in backscattered-electron morphologies (A in Fig.4(d)) had a lower average atomic weight in comparison to the white regions (B in Fig.4(d)). Results of EDS analyses (Fig.4(e) and Fig.4(f)) showed that the dark regions had higher Al content, i.e. thicker alumina overlay, than white region. This result indicated the thickness of alumina overlay was not uniform probably due to the rough character of the YSZ surface.

The cross-section of the YSZ with alumina overlay is shown in Fig.5. The thickness of alumina overlay was ranged from 100nm to 500nm. Occupation of the microcracks and porous near the surface in YSZ by alumina because of penetration of the low viscosity precursor could also be found (as shown in Fig.5 by arrows).

4.2 XRD and SEM analyses on TBC and TBC/Al_2O_3 samples by PVD and HVOF

X-ray diffraction before and after exposure to molten slats has provided the information of the extent of reactions occurred during hot corrosion in TBC. The X-ray diffraction of as-sprayed TBC demonstrated that it contained predominantly T-phase of ZrO_2 (A in Fig.6). After exposure to the molten mixture of salts of Na_2SO_4 + 5%V_2O_5 at 950^oC for 10h, the XRD patterns (B in Fig.6) showed that corresponding to a remarkable decrease in intensity of T-phase of zirconia, a substantial amount of M-phase was formed due to the leaching of Y_2O_3 from YSZ resulting from the reaction of Y_2O_3 with V_2O_5 to form YVO_4 (which was found in XRD patterns) according the reaction (1) indicated in Introduction.

For the TBC/EB-PVD overlay Al_2O_3 coating system, the XRD patterns after exposure to molten slats (B in Fig.7) showed a few amount of M-phase in the specimen and no YVO_4 peaks could be detected. Overlay Al_2O_3 coating had undergone structure change from $g-Al_2O_3$ crystalline $a-Al_2O_3$. However, no reaction products between Al_2O_3 and mixed molten salts could be identified from the XRD results. From the XRD patterns of the sample whose Al_2O_3 coating was partially removed before XRD analyses, as shown in C in Fig.7, it can be found that remarkable increase in the intensity of T-phase was resulted, indicating the destabilization (D) of the TBC with overlay Al_2O_3 coating was much lower than that of TBC without overlay coating. Namely the attack of YSZ by molten salts was limited due to the present of Al_2O_3 overlay coating.

Similarly, B in Fig.8 shows the XRD patterns of TBC with HVOF Al_2O_3 coating after exposure. It was quite notable that just a little bit amount of M-phase was formed after exposure to molten salts. YVO_4 was not picked up by XRD in the specimen, probably due to its low content that was below the detection limit. A large amount of g - Al_2O_3 was transformed to a - Al_2O_3 after subjecting to hot corrosion at high temperature.

Based on the XRD results, destabilization (D) could be obtained for different TBC system, as demonstrated in Fig.9. It clearly showed that Al_2O_3 overlay coating can prevent the YSZ from hot corrosion by molten salts containing vanadium.

4.3 SEM observation

4.3.1 Conventional YSZ TBC

For conventional YSZ TBC system, after exposure to the salts, characteristic surface crystals among the fine zirconia grain were formed which was rich in yttrium (40.53at%) and

vanadium (36.31at%) and contained no zirconium (Fig.10). The essentially equal amounts of yttrium and vanadium indicated the crystal on the surface of TBC to be YVO_4. This was consistent with the results of XRD analyses in which the peaks of YVO_4 were clearly shown. From SEM micro images of cross-section (Fig.11), it was found that YVO_4 existed not only near the surface of TBC but also in the area near the bond coat, indicating that molten salts has deeply penetrated into the TBC along the porous and cracks.

X-ray maps of the cross-section of YSZ coating after a hot corrosion test are shown in Fig.12. Defects, such as pores and cracks, were observed along the cross-section. Sulphur, but no sodium, has been found in the interface region between the bond coat and substrate. Because the sample after exposure had been washed in water, sulphur was considered to come from sulphide, such as FeS, which can't be dissolved by water, as suggested by Chen et al [6]. Vanadium could not be detected in this magnification, probably due to its low content that was below the detection limit. In addition, it can be seen that the bond coat has been visibly oxidized after exposure.

4.3.2 TBC/EB-PVD overlay Al_2O_3 coating

In the new TBC system that has overlay of Al_2O_3 coating deposited by EB-PVD, the surface morphology was transformed to uniformly faceted shape after exposure due to the formation and growth of $\alpha - Al_2O_3$ crystal (Fig.13(a)). In addition, there were crystallites marked with A in Fig.13(b) that grew along a preferred direction. By EDX analyses, it was found that they contained O, Na, Al and S, as show in Fig.13(c). These crystallites were considered to be $NaAlO_2$ that seemed to be dense, as suggested by Chen et al [6]. However, the morphology of $NaAlO_2$ crystallites were different from that described in literature [6] where $NaAlO_2$ covered the APS sprayed Al_2O_3 coating. Due to partially spallation of Al_2O_3 grains, fine zirconia grains beneath the alumina cover layer could also be found on the surface in some large interspaces between alumina grains, as shown in Fig.13(d). However, it seemed that there was no evidence of the reaction between Al_2O_3 and V_2O_5.

X-ray maps of cross-section of YSZ/EB-PVD Al_2O_3 coating after exposure are shown in Fig.14. The thickness of Al_2O_3 coating after exposure was about the same as that of as-deposited coating. Although Al_2O_3 layer was less dense comparing to the layer before exposure because of the presence of interspaces between Al_2O_3 grains and cracks in the Al_2O_3 overlay and at the interface between Al_2O_3 overlay and the TBC, sulpure could not be found along the cross-section maps. Moreover, less oxidation of the bond coat was observed.

4.3.3 TBC/HVOF overlay Al_2O_3 coating

In the case of TBC system that has overlay Al_2O_3 coating sprayed by HVOF, the surface was still dense even after exposure to the molten salts for 10h at 950°C, as shown in Fig.15. It is quite notable that the microstructure of the surface did not have notable variation compared with that of as-sprayed specimen, although it has been translated to α - Al_2O_3 from γ -Al_2O_3. The much less formation of M-phase revealed the excellent barrier action of alumina layer sprayed by HVOF to prevent the TBC from the attack of molten salts.

X-ray maps of cross-section of YSZ/HVOF Al_2O_3 coating after exposure are shown in Fig.16. Obviously, Al_2O_3 overlay sprayed by HVOF was denser than that deposited by EB-PVD after exposure. Also, there was no distinct change for HVOF Al_2O_3 overlay before and after exposure. Accordingly, HVOF Al_2O_3 overlay is more effective in preventing the TBC from the attack by molten salts.

4.3.4 TBC/CSG overlay Al_2O_3 coating

X-ray diffraction analysis was performed on the specimen before and after hot corrosion testing. The X-ray diffraction pattern of the as-sprayed YSZ TBC demonstrated that it contained predominantly T-phase of ZrO_2 (Pattern A in Fig.17). After exposure to the molten salts at 950^{o}C for 10 h, high YVO_4 peaks was found in XRD analyses (Pattern B in Fig.17), implying the leaching of Y_2O_3 from YSZ by the reaction of Y_2O_3 with V_2O_5 or $NaVO_3$. As a result, the intensity of T-phase remarkable decreased, and a substantial amount of M-phase was formed due to the leaching of Y_2O_3 from YSZ. This was in agreement with previous investigation on hot corrosion of YSZ coating [1-2].

Fig.18 exhibited the XRD patterns of the YSZ/Al_2O_3 system before and after hot corrosion testing. The X-ray beam of the XRD diffractometer was focused on the surface of the Al_2O_3 overlay and corresponding results were shown in Pattern A and B in Fig.18. The Al_2O_3 overlay after calcined at 1200^{o}C showed the α-phase structure (Pattern A in Fig.18). After exposure to the molten salt, the results showed that the T-phase of ZrO_2 in the YSZ coating was still predominant (Pattern B in Fig.18). And a little amount of the M-phase of ZrO_2 and YVO_4 existed in the YSZ coating. It is worth to notice that peaks correspond to α- Al_2O_3 were still evident, indicating no evidence that the chemical reaction of the Al_2O_3 overlay with the molten salt had taken place. However, a peak with the *d* value of 2.445A (as shown by arrow in Fig.18) could be found on the corroded YSZ/Al_2O_3 sample, which was considered to be $CoAl_2O_4$ phase and will be discussed when SEM results are presented.

Visual examination of the surface of YSZ/Al_2O_3 coating found that the surface was white before corrosion and it became blue after corrosion. Further SEM examination results are shown in Fig.19. It can be seen that Al_2O_3 overlay still covered the almost YSZ surface, but the crystals of Al_2O_3 were coarser and less dense than those before exposure (Fig.19(a) and Fig.4(b)). Trace of Na was detected on coarser Al_2O_3 crystals region. In some regions, however, coarse and faceted crystals which filled in the porous and cracks on the YSZ surface were observed (Fig.19(b)). Those crystals consisted of Al, Co and O as well as a few Cr and Zr. The YSZ coating around those crystals was visible. Quantitative EDS analyses indicated those crystals contained 53at.%O, 28at.%Al and 14at.%Co. As a result, those crystals were identified to be $CoAl_2O_4$. $CoAl_2O_4$ could also be found in XRD analyses in Fig.18, which corresponded to the peak marked with arrow.

Fig.20 demonstrates the cross-section of composite YSZ/Al_2O_3 system after 10 h of exposure. Consistence with the surface morphology, alumina overlay was still adherent to the YSZ (Fig.20(a)). It is worthy of noticing that some of the pores and cracks within the YSZ coating were filled by $CoAl_2O_4$ (marked by arrows in Fig.20(b)), which was confirmed by the EDS analysis.

4.4 SIMS analyses

In order to detect the vanadium within TBC, The TRIFT TOF-SIMS was used. The primary ions were delivered using a 15keV liquid metal (Ga^+) ion gun with a beam current 600pA. The primary ions were focused on the YSZ layer in cross-section sample with a raster

size of $600\times600\,mm^2$. The spectrum was acquired using a total ion dose of 1×10^{12} ions/cm^2. The result of SIMS is shown in Table1.

Table 1 Quantitatively comparison of vanadium content in the YSZ layer by SIMS

	YSZ	YSZ/EB-PVD Al_2O_3	YSZ/HVOF Al_2O_3
V/Zr	0.1	0.016	0.014

It was clearly showed that Al2O3 overlay coating significantly decreased vanadium content, which is a reflection of YVO4 formed in YSZ.

The main problem associated with the Al_2O_3 overlay is the cracking of alumina coating during hot corrosion tests. The reason for the formation of cracks was considered to be (1) the conversion to crystal $\alpha-Al_2O_3$ from γ - Al_2O_3 is associated with a volume shrinkage that easily causes internal cracking; (2) the heating cycle causes tensile stresses in the alumina due to the mismatch in thermal expansion coefficient (TEC) between alumina (TEC $\approx 8-9\times10^{-6}/^oC$) and zirconia (TEC $\approx 11-13\times10^{-6}/^oC$), which will very easily crack under this tensile straining.

4.5 Indentation tests: Effect of overlay thickness on stress in YSZ coating and spalling of YSZ coating

To improve the hot corrosion resistance of YSZ thermal barrier coatings, a 25 mm and a 2 mm thick Al_2O_3 overlay were deposited by HVOF thermal spray and by sol-gel coating method, respectively, onto to the surface of YSZ coating. Indenter test was employed to investigate the spalling of YSZ with and without Al_2O_3 overlay after hot corrosion. The results showed that Al_2O_3 overlay acted as a barrier against the infiltration of the molten salt into the YSZ coating during exposure, thus significantly reduced the amount of M-phase of ZrO_2 in YSZ coating. However, a thick Al_2O_3 overlay was harmful for TBC by increasing compressive stress which causes crack and spalling of YSZ coating. As a result, a dense and thin Al_2O_3 overlay is critical for simultaneously preventing YSZ from hot corrosion and spalling.

Trying to measure the YSZ/bond coat interfacial toughness lose after hot corrosion using indentation test proposed by A. Vasinonta et al [7] was failed due to much thick YSZ coating employed in the present work. For such thick YSZ, buckling never occurred during indenter test because the indenter could not throughout penetrate the YSZ coating and as a result, interface crack could not be driven by the compressive radial strains. Nevertheless, a much large compressive stress could be induced through the YSZ coating thickness during indenter test. The compressive stresses induced by indenter and due to the phase transformation of T$\rightarrow$M were very harmful for the coating spalling.

After hot corrosion for 10 h and 100 h, visual and SEM examination showed no cracks on the YSZ surface and spalling for monolithic YSZ TBC system. On the contrary, composite YSZ/Al_2O_3 (25 mm) system showed the formation of cracks and spalling of YSZ after hot corrosion for ~100 h, as shown in Fig.21. This result demonstrated that Al_2O_3 overlay increased the compressive stress within the YSZ coating due to mismatch in thermal expansion between Al_2O_3 and YSZ. It is further evidenced by the indenter test results, as shown in Fig.22. As can be seen from Fig.22, for 10 h hot corrosion, monolithic YSZ system did not show cracking and spalling, whereas spalling was clearly observed on the YSZ/Al_2O_3 (25 mm) system.

Furthermore, after 100 h hot corrosion, monolithic YSZ system only cracked during indenter test, while spalling and cracking occurred on the YSZ/Al_2O_3 (25 mm) system. Instead of thick Al_2O_3 overlay, however, when much thin Al_2O_3 overlay (2 mm) was deposited, neither crack nor spalling could be found on the sample hot corroded for ~100 h during indenter test, as demonstrated in Fig.23. These results revealed that a dense and thin Al_2O_3 overlay is critical for simultaneously preventing YSZ TBC from attack of molten salt and spalling caused by compressive stress.

It is known that phase transformation from T-phase to M-phase of ZrO_2 is accompanied by a large destructive volume change, which will induces much large compressive stress within the YSZ coating. However, the results mentioned above demonstrate that the stresses developed in monolithic YSZ coating after hot corrosion are not sufficient to cause failure, although a large amount of M-phase of ZrO_2 was formed due to hot corrosion. On the other hand, composite YSZ/Al_2O_3 (25 mm) overlay TBC system showed early failure through delamination. The mechanisms leading to delamination are what must be addressed.

Due to thermal expansion mismatch between Al_2O_3 overlay and YSZ coating, stresses developed on cooling can lead to spalling or delamination of YSZ coating. The stress caused by the thermal expansion is formulated by

$$\sigma_{YSZ} = \frac{E_a' \times E' \times H_a}{E_a' \times H_a + E' \times H}(\alpha_a - \alpha) \times \Delta T \qquad (3)$$

$$\sigma_a = \frac{E_a' \times E' \times H}{E_a' \times H_a + E' \times H}(\alpha - \alpha_a) \times \Delta T \qquad (4)$$

where, $E_a' = E_a/(1-\nu_a)$, and $E' = E/(1-\nu)$. E, ν and α are Young's modulus, Poisson's ratio, and thermal expansion coefficient of the YSZ coating respectively; E_a, ν_a and α_a are Young's modulus, Poisson's ratio, and thermal expansion coefficient of Al_2O_3 overlay respectively; H and H_a are the thickness of YSZ coating and Al_2O_3 overlay, respectively. The Young's modulus of YSZ is 50 GPa and that of Al_2O_3 overlay is 375 GPa. ν and ν_a are supposed to be 0.1 and 0.25 respectively. α and α_a are 11×10^{-6} and 8×10^{-6}, respectively. ΔT, difference between exposure temperature and room temperature after cooling, can be taken as -930°C (950°C-20°C). Thus the stresses encountered in YSZ coating on cooling to room temperature are approximately 73.35MPa and 10.4MPa for Al_2O_3 overlay thickness of 25 mm and 2 mm, respectively. It clearly shows that the effect of Al_2O_3 overlay on the residual stress in YSZ coating can be significantly reduced when a much thin overlay is deposited. Similarly, the stress in Al_2O_3 overlay after cooling can be estimated to be -734MPa and -1300MPa, for Al_2O_3 overlay thickness of 25 mm and 2 mm, respectively.

Upon cooling, planar stress states will be developed in the YSZ coating due to CTE mismatch between the YSZ coating and the bond coat, and Al_2O_3 overlay, causing spalling of the YSZ coating. Based upon the above stresses estimation, a tensile stress was developed in YSZ coating near the YSZ/Al_2O_3 overlay interface after cooling due to the presence of Al_2O_3 overlay. It might be found that the compressive stress with in the YSZ coating could be increased due to this tensile stress. As the Al_2O_3 overlay thickness was decreased to 2 mm, the

effect of Al_2O_3 overlay on the compressive stress could be negligible. Consequently, the spalling of YSZ coating due to the presence of Al_2O_3 overlay can be minimized.

5. CONCLUSION

Overlay Al_2O_3 coatings with 0.1~ 25 *mm* thickness have been successfully deposited on TBC by EB-PVD, HVOF and composite-sol-gel (CSG) techniques. It has been found that overlay Al_2O_3 coatings were dense, continues and adherent to the TBC. In hot corrosion tests, Al_2O_3 coating rarely reacted with the molten salts. After exposure to the molten Na_2SO_4 + 5%V_2O_5 salts, just a few M-phase of zirconia was formed and no YVO_4 could be detected comparing to the conventional TBC system. As a result, Al_2O_3 coating play a key role in preventing the TBC from the attack by molten salts, although there were some cracks in overlay Al_2O_3 coating and at the Al_2O_3/TBC interface formed during hot corrosion tests.

Because of thin and dense CSG alumina overlay on the YSZ surface and occupation of the microcracks and porous near the surface in YSZ by alumina resulting from the penetration of the low viscosity CSG precursor, the infiltration of the molten salt into the YSZ coating was remarkably refrained. After hot corrosion, the amount of M-phase in the TBC coating with Al_2O_3 overlay was substantially reduced comparing with that without the Al_2O_3 overlay.

Indenter test was employed to investigate the spalling of YSZ with and without HVOF and CSG Al_2O_3 overlay after hot corrosion test. A thick Al_2O_3 overlay was harmful for TBC by increasing compressive stress which causes crack and spalling of YSZ coating. As a result, a dense and thin Al_2O_3 overlay is critical for simultaneously preventing YSZ from hot corrosion and spalling.

6. PAPER PUBLISHED:

- Z. Chen, N. Wu and S X. Mao, "Hot Corrosion Mechanism of Composite Alumina/Yttria-Stabilized Zirconia Coating in Molten Sulfate-Vanadate Salt", ***Journal of the American Ceramic Society,*** 457, p.301-306 (2004).

- Z. Chen, N. Wu, J. Singh, S X. Mao, "Effect of Al_2O_3 Overlay on hot-corrosion behavior of yttria-stabilized zirconia coating in molten sulfate-vanadate salt", ***Solid Thin Film*** 443,pp46-52 (2003).

7. REFERENCES

[1] I.Gurrappa. Thermal barrier coating for hot corrosion resistance of CM 247 LC superalloy. J. Mater.Sci.Lett., 17(1998)1267-1269

[2] R.L.Jones. Thermogravimetric study of the 800 **degree** reaction of zirconia stabilizing oxides with SO_3-$NaVO_3$. J. Electrochem.Soc., 1992, 10(39)2794-2799

[3] R.L.Jones. India as a hot corrosion-resistant stabilizer for zirconia. J.Am.Ceram.Soc., 1992, 75(7)1818-1821

[4] S.A.Muqtader and R.K.Sidhu. Destabilization behavior of ceria-stabilized tetragonal zirconia polycrystals by sodium sulphate and vanadium oxide melts. J.Mater.Sci.Lett., 12(1993)831-833

[5] A.Rabiei and A.G.Evans. Failure mechanisms associated with the thermally grown oxide in plasma-sprayed thermal barrier coatings. Acta Materialia. 48(2000)3963-3967

[6] H.C.Chen et al. Degradation of plasma-sprayed alumina and zirconia coatings on stainless stell during thermal cycling and hot corrosion. Thin solid films. 223(1992)56-64

[7] Aditad Vasinonta and Jack L. Beuth, "Measurement of interfacial toughness in thermal barrier coating systems by indentation", 68, 843-860(2001).

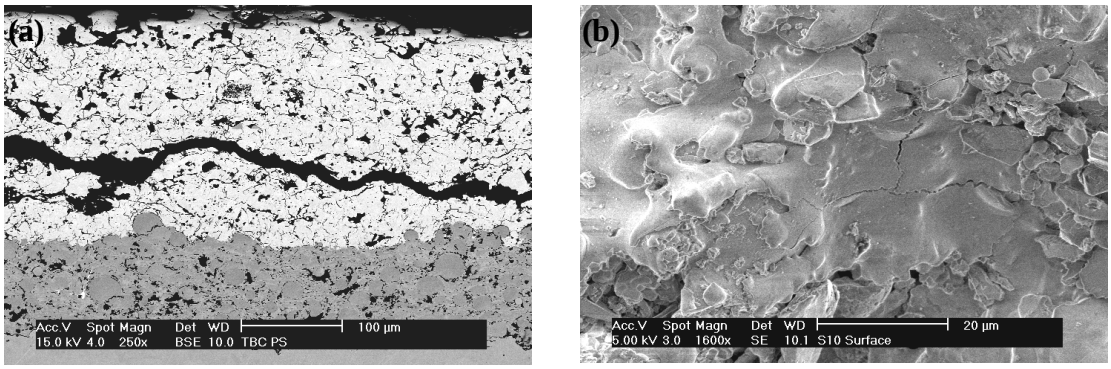

Fig.1 SEM micrographs of (a) cross-section and (b) surface of as-sprayed TBC

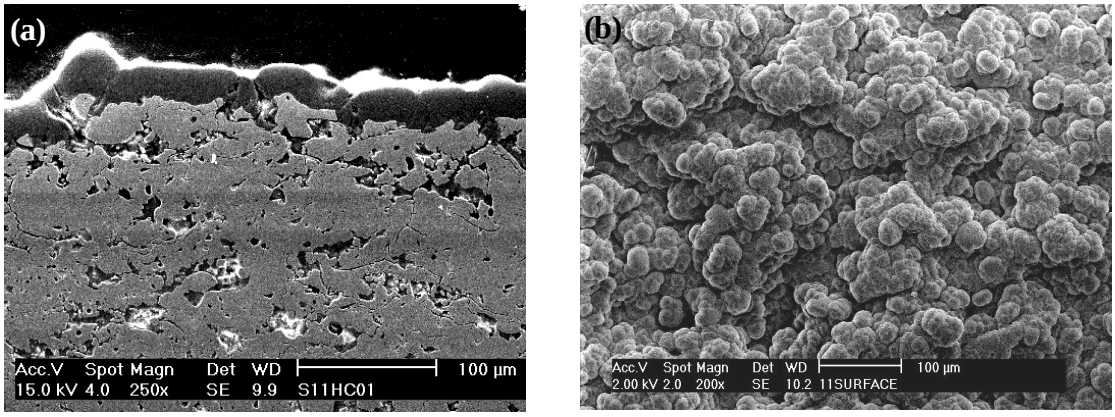

Fig.2 SEM micrographs of (a) cross-section and (b) surface of TBC with EB-PVD overlay Al_2O_3 coating

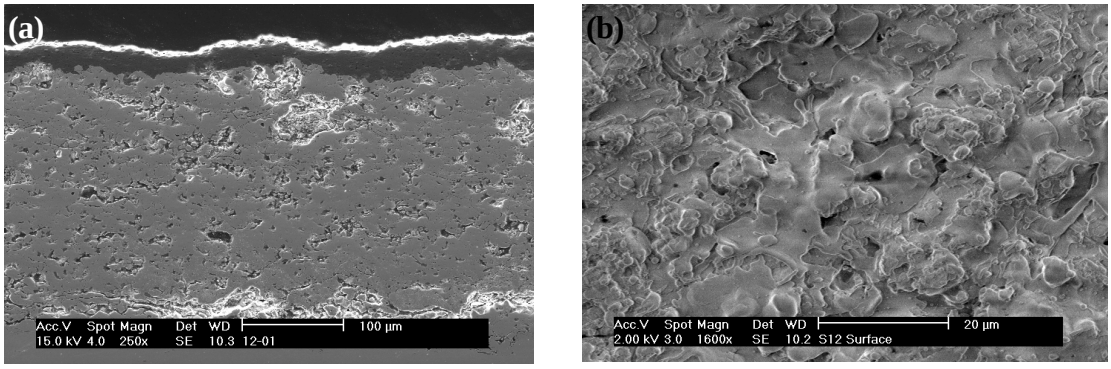

Fig.3 SEM micrographs of (a) cross-section and (b) surface of TBC with HVOF overlay Al_2O_3 coating

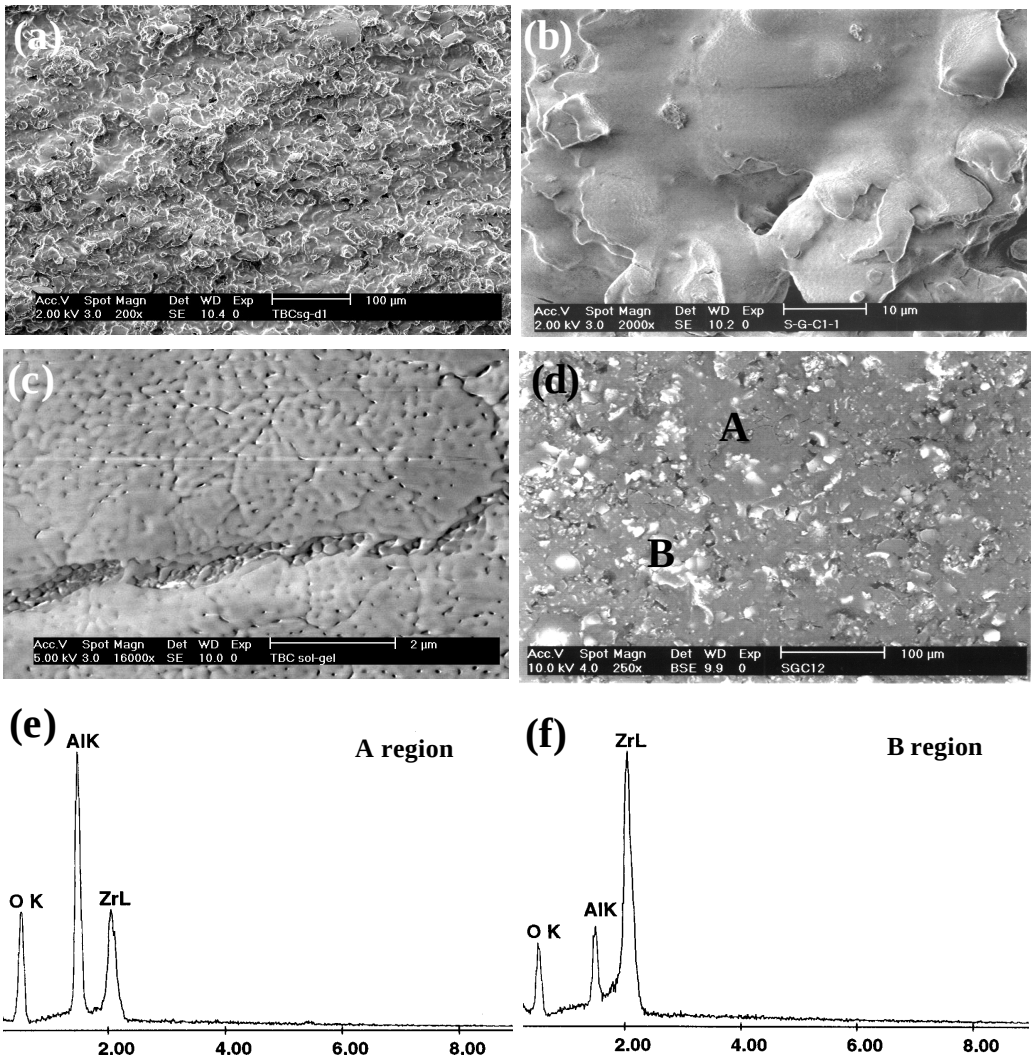

Fig.4 Surface morphology of YSZ deposited with CSG alumina coating

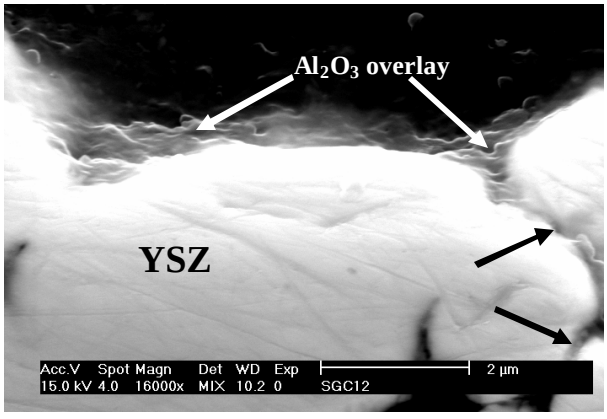

Fig.5 Cross-section of YSZ with CSG alumina overlay

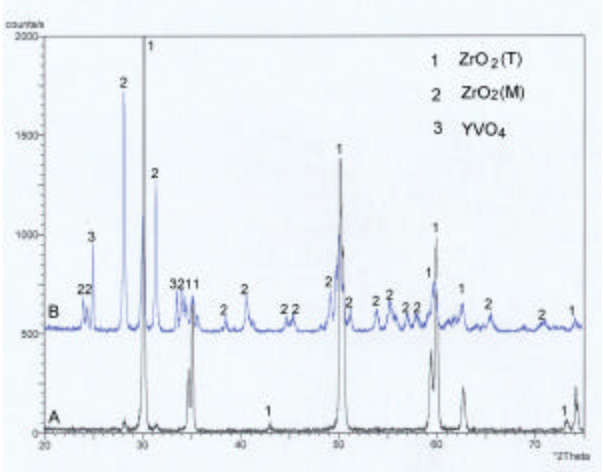

Fig.6 XRD patterns of TBC before and after exposure to the molten salts

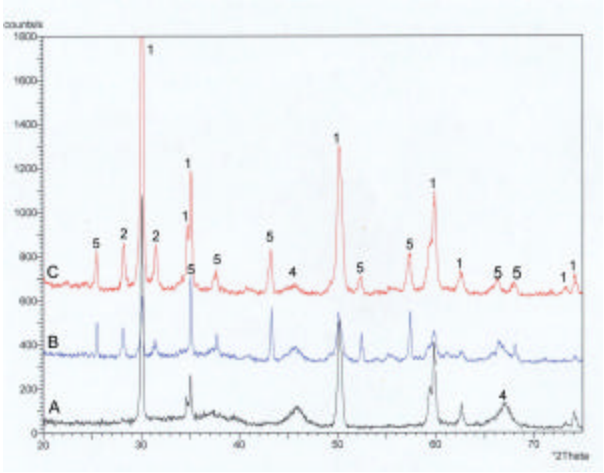

Fig.7 XRD patterns of TBC with EB-PVD Al_2O_3 overlay coating before and after exposure to the molten salts(4: g -Al_2O_3, 5: α-Al_2O_3)

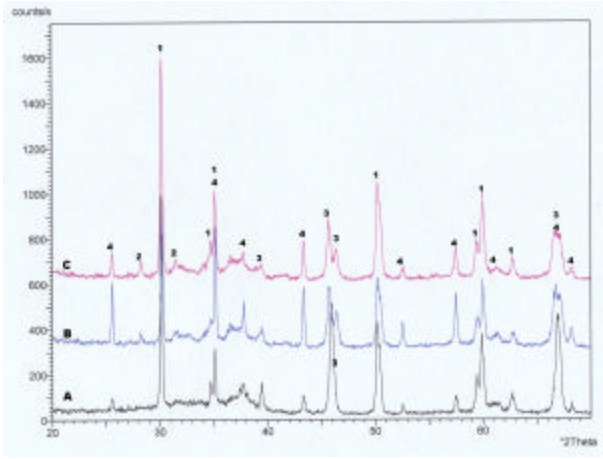

Fig.8 XRD patterns of TBC with HVOF Al_2O_3 overlay coating before and after exposure (A: TBC with as-deposited overlay Al_2O_3 ; B: after exposure; C: after partially removing Al_2O_3 overlay after exposure)

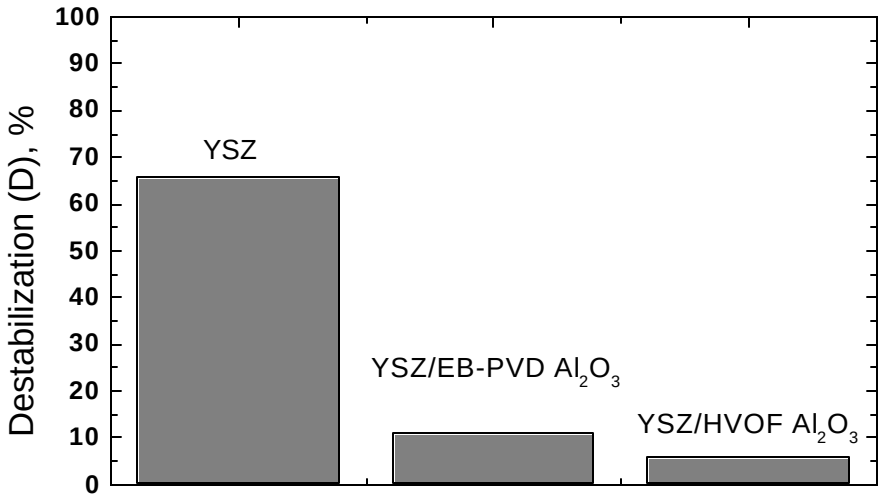

Fig.9 A comparing in destabilization (D) of the TBC with and without overlay Al_2O_3 coating

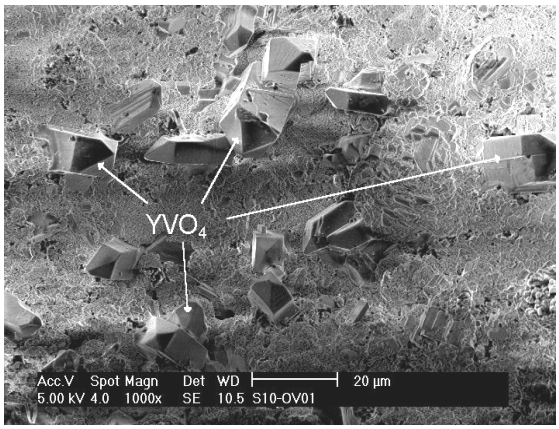

Fig.10 SEM surface micrograph of TBC after exposure showing the formation of YVO_4

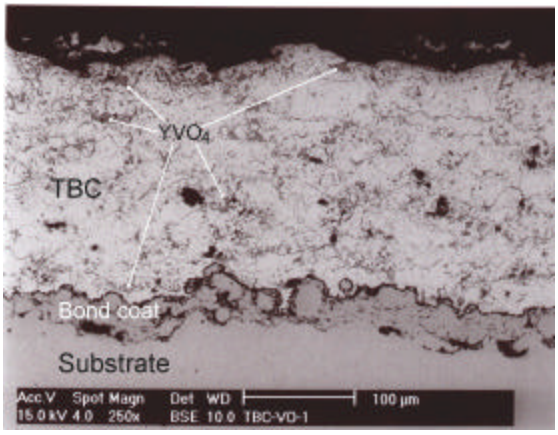

Fig.11 SEM microimages of cross-section of TBC after exposure

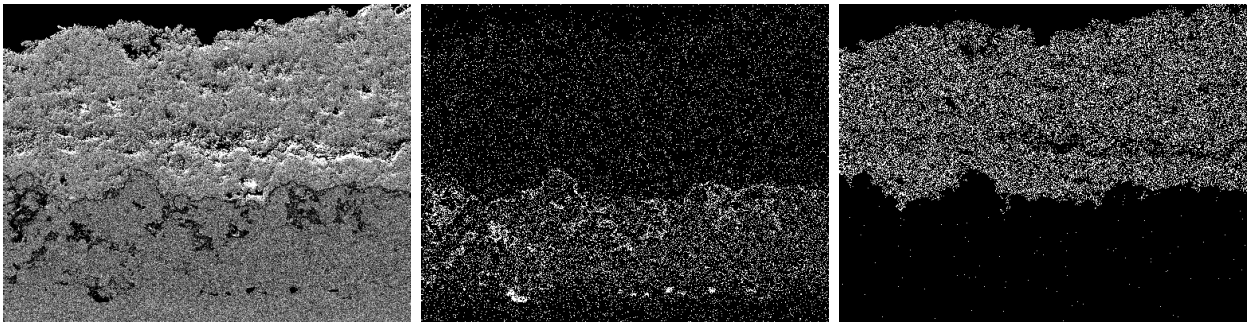

SEM of YSZ Al Zr

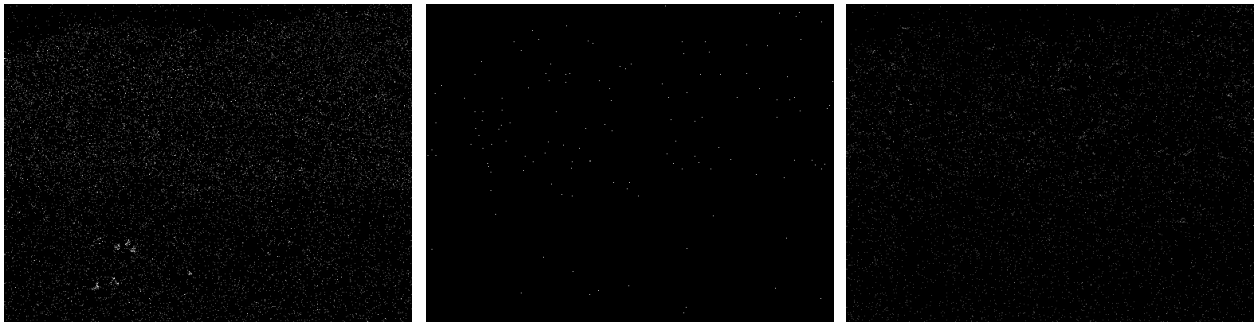

S Na V

Fig.12 X-ray maps of the cross-section of YSZ coating after a hot corrosion test

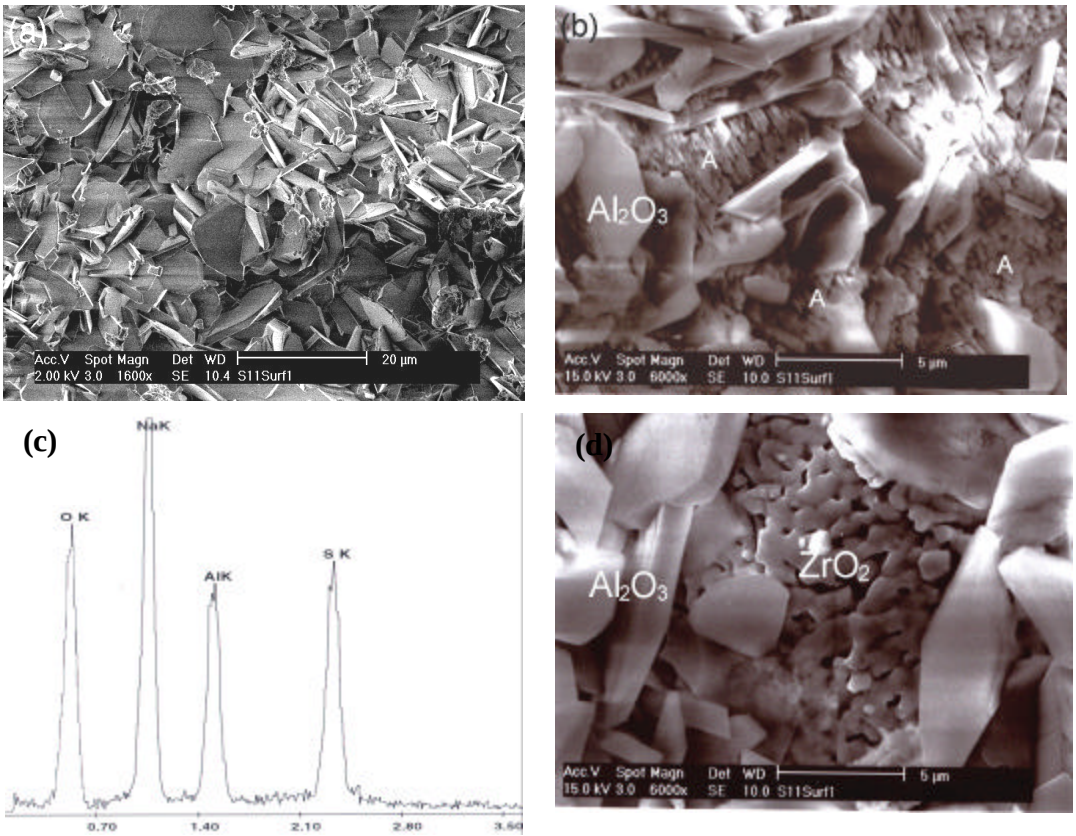

Fig.13 Surface micrograph of YSZ/EB-PVD Al_2O_3 coating after exposure to the molten salts

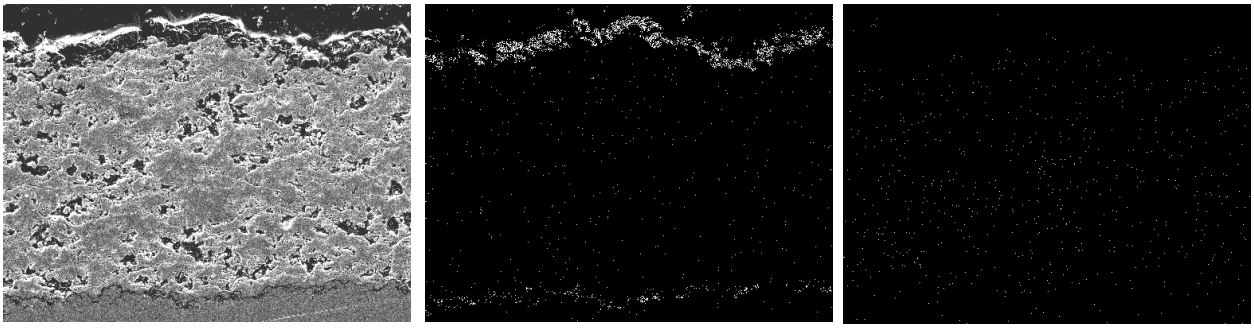

SEM Al S

Fig.14 X-ray maps of cross-section of YSZ/EB-PVD Al_2O_3 coating after exposure

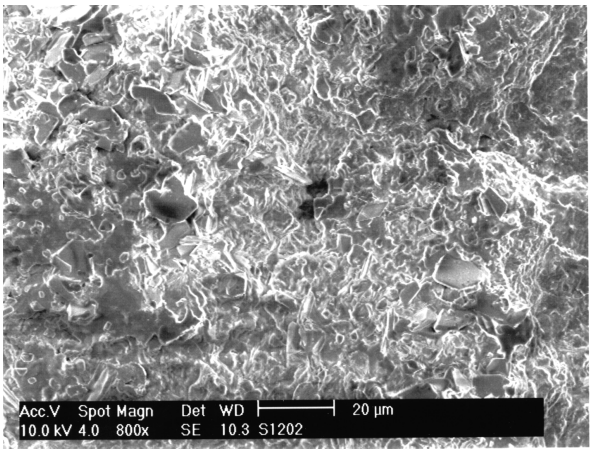

Fig.15 Surface SEM micrograph of HVOF overlay coating after exposure to the salts

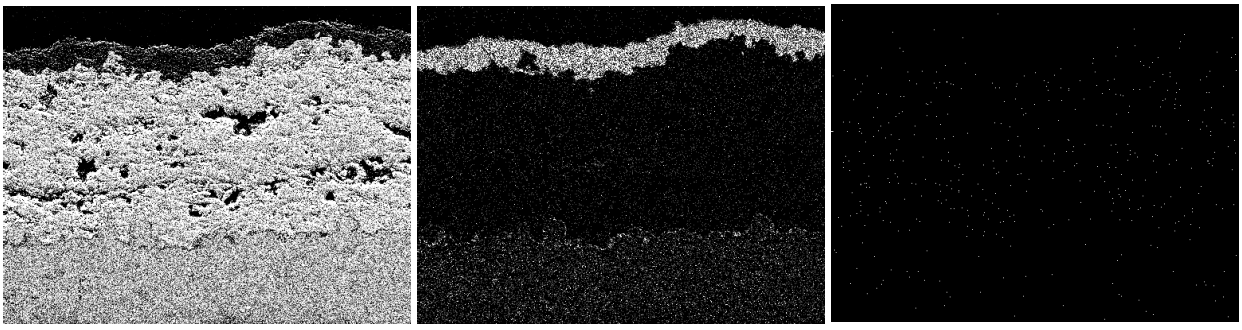

SEM Al S

Fig.16 X-ray maps of cross-section of YSZ/HVOF Al_2O_3 coating

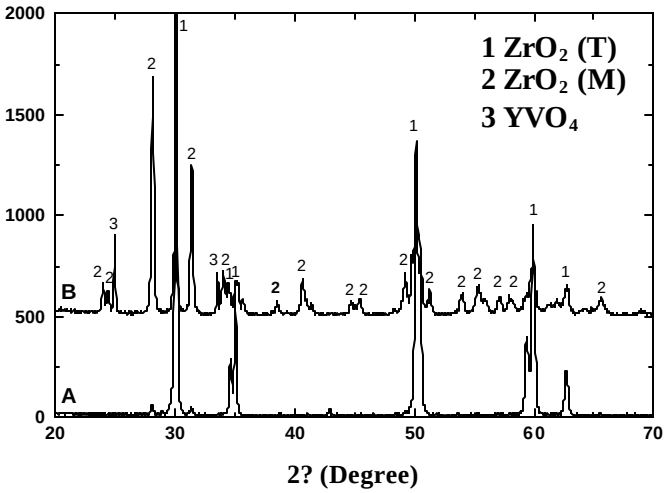

Fig.17 XRD patterns of TBC before exposure (A) and after exposure (B) to the molten salts

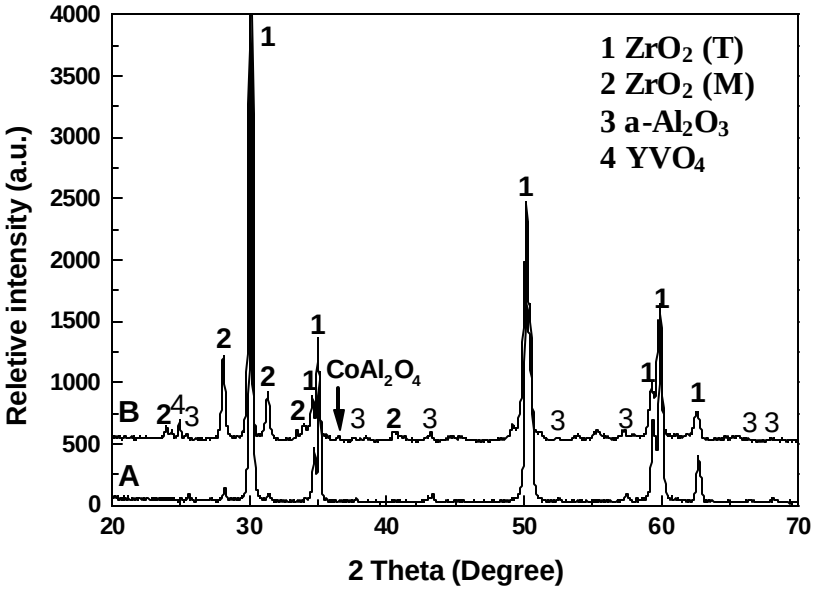

Fig.18 XRD patterns of YSZ coated with CSG alumina overlay before exposure (A) and after exposure (B) to the molten salts

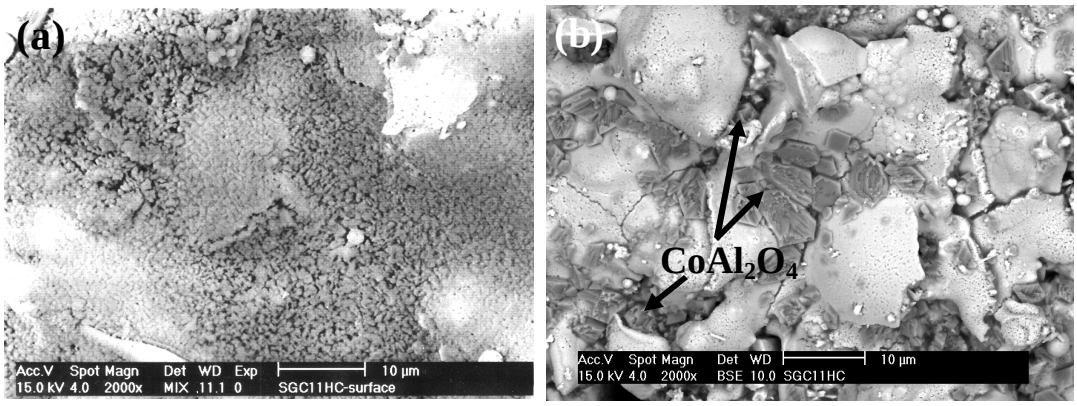

Fig.19 Surface photographs of YSZ with CSG alumina overlay after exposure

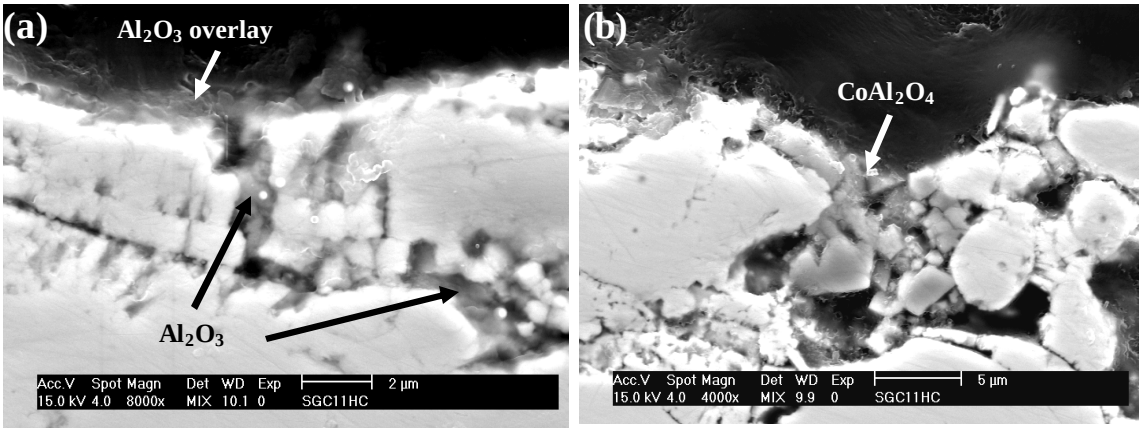

Fig.20 Cross-section of YSZ with CSG alumina overlay after exposure

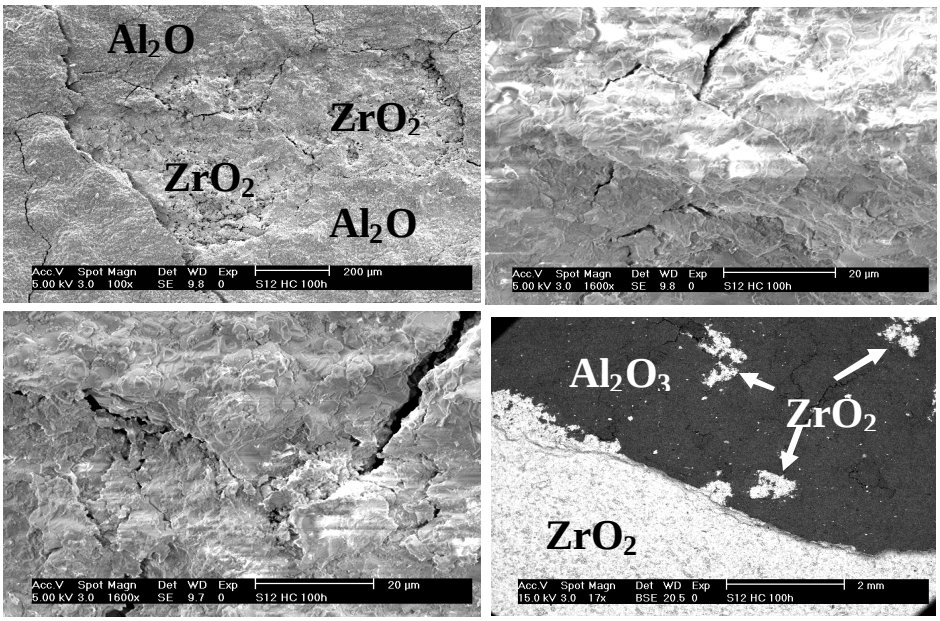

Fig.21 SEM images showing the formation of cracks and spalling of YSZ after hot corrosion for ~100 h in composite YSZ/Al_2O_3 overlay (25 *mm*) system.

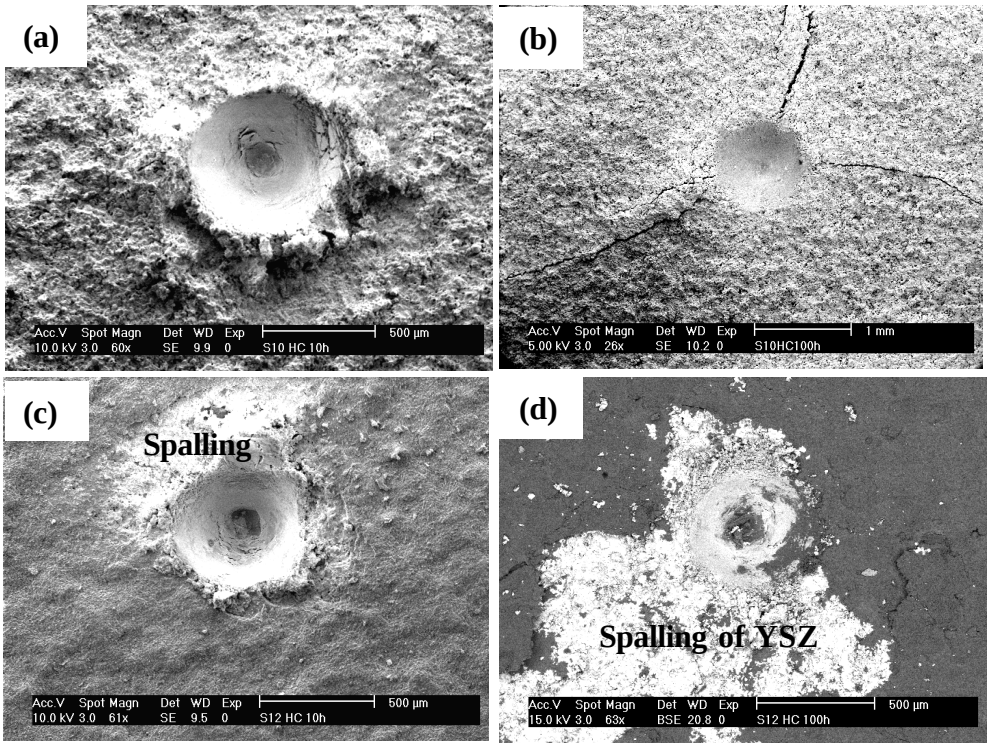

Fig.22 Cracking and spalling of YSZ coating with and without Al_2O_3 (25 *mm*) after hot corrosion during indenter test.(a) and (b)YSZ,10h and 100h; (c) and (d)YSZ/Al_2O_3 (25 *mm*), 10h and 100h

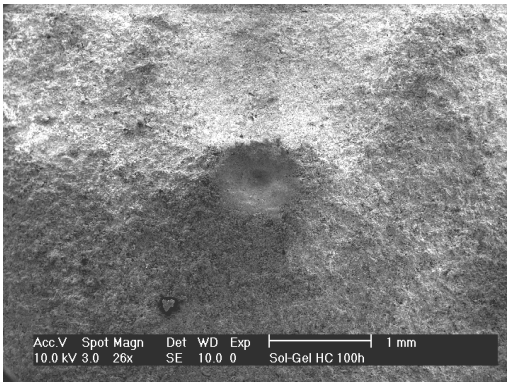

Fig.23 SEM image showing no cracks and spalling of YSZ in YSZ/Al_2O_3 overlay(2 mm) system after hot corrosion of 100 h.